

Mechanical Strength of Thermally Aged Sn-3.5Ag/Ni-P Solder Joints

M. HE, Z. CHEN, and G.J. QI

This work presents an investigation on the influence of the solder/under bump metallization (UBM) interfacial reaction to the tensile strength and fracture behavior of Sn-3.5Ag/Ni-P solder joints under different thermal aging conditions. The tensile strength of Sn-3.5Ag/Ni-P solder joints decreases with aging temperature and duration. Four types of failure modes have been identified. The failure modes shift from the bulk solder failure mode in the as-soldered condition toward the interfacial failure modes. Kirkendall voids do not appear to affect the tensile strength of the joint. The volume change of Ni-P phase transformation during the thermal aging process generates high tensile stress inside the Ni-P layer; this stress causes mudflat cracks on the remaining Ni-P coating and also leads to its delamination from the underlying Ni substrate. In general, interfacial reaction and the subsequent growth of Ni_3Sn_4 intermetallic compound (IMC) layer during solid-state reaction are the main reasons for the decrease of tensile strength of the solder joints. The current study finds there is an empirical linear relation between the solder joint strength and the Ni_3Sn_4 intermetallic compound (IMC) thickness. Therefore, the IMC thickness may be used as an indication of the joint strength.

I. INTRODUCTION

THE interfacial reaction between solder and solderable base metal is often an indication of sound wetting and the formation of a metallurgical bond. A solder joint consists of the solder, the base metal, and the interfacial layer(s), each with its own unique properties. The mechanical properties of the solder joint depend on each of the three primary structures. The thickness of the intermetallic compound (IMC) layer, which is produced in most of the soldering processes, ranges normally from 1 to 3 μm with different process conditions.^[1] It increases with the reaction time of molten solder with the solderable coatings and further with the progress of solid-state diffusion, after the solder joint has solidified.^[2-7] The excessive growth of intermetallic compounds may be detrimental to the reliability of the solder joint because of the brittleness of the intermetallic layer, and the stress concentration generated from the volume change or complete consumption of the solderable coating. Thus, it is important to study the mechanical strength of the solder joints in relation to the presence of IMCs.

Numerous studies have examined the IMC growth kinetics and the fracture behavior of solder joints formed by Sn-bearing solders and copper metallization.^[4,5,8-11] For the Ni-based UBM systems, Frear *et al.*^[12] found that fracture occurred through the interfacial Ni_3Sn_4 IMC layer formed between Sn-40Pb solder and Ni substrate in all the IMC thicknesses investigated. For Sn/Ni and Sn-0.7Cu/Ni solder joints, the joint tensile strength decreased with extended reaction time, while the fracture path shifted from the bulk solder toward the intermetallic layer.^[13] Owing to the presence of P, the reaction between Sn and Ni-P is more complicated than that between Sn and pure

Ni. Besides the existence of the Ni_3Sn_4 layer, the formation of additional layers, such as the Ni-Sn-P^[3,14-16] and the Ni_3P layers,^[17,18] may influence the fracture behavior of the solder joint. The residual stresses at the interfaces are more complicated with the presence of these multilayers. In a solder/Ni-P joint failure, shear test found that fracture initiation was either reported to be inside the eutectic solder,^[19] or inside the Ni_3Sn_4 and Ni_3P layers,^[20] or at the Ni-P/substrate interface.^[19] Chonan *et al.* reported that the cold bump pull strength decreased when P concentration increased. Failure was reported to occur partially inside the P-rich layer in the liquid state reaction process.^[21,22] Among these limited reports on solder/Ni-P joint failure, the difference in strength and fracture path might be due to the fact that different researchers employed different process conditions in their studies. A thorough investigation would require a wider processing window that corresponds to a larger variation of the interfacial conditions.

Ni_3Sn_4 IMC growth kinetics in the solid state of the Sn-3.5Ag/Ni-P joint has been extensively discussed in our previous work.^[3] The present work will focus on the mechanical testing and fracture behavior of solder joints at different thermal aging conditions. The objective is to establish a correlation between microstructure and mechanical properties of the solder joint formed between Sn-3.5Ag and electroless Ni-P alloy. To this aim, the tensile strength of the Sn-3.5Ag/Ni-P solder joint was measured under different thermal aging temperatures ranging from 150 °C to 216 °C. Varying the aging time at each temperature enables a wide spectrum of interfacial microstructures to be produced: from the ones close to production/usage to the extreme ones that are less often encountered in reality. The fracture behavior of the solder joint has been understood from the perspectives of microstructural evolution and its related interfacial stresses.

II. EXPERIMENTAL PROCEDURES

Nickel (99 pct) plates, measuring $12.5 \times 8.0 \times 2.0$ mm, were used as substrate for the plating of electroless nickel.

MIN HE, Ph.D. Candidate, and ZHONG CHEN, Associate Professor, are with the School of Materials Engineering, Nanyang Technological University, Singapore 639 798. Contact e-mail: aszchen@ntu.edu.sg GUOJUN QI, Senior Scientist, is with the Singapore Institute of Manufacturing Technology, Singapore 638 075.

Manuscript submitted May 31, 2004.

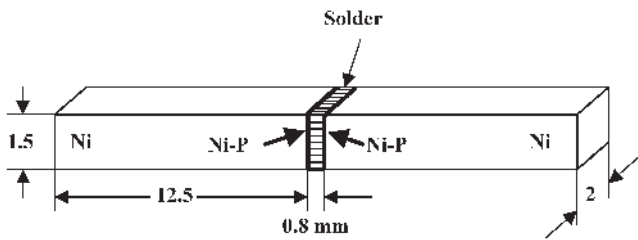


Fig. 1—Dimensions of the tensile testing specimen used in this study. The dimensions are in millimeters.

The plates were polished to an optical finish on the 8.0×2.0 mm surfaces, and then solvent degreased and rinsed in deionized water before subsequent electroless nickel plating. A Ni-P (7 wt pct P) layer of about $5 \mu\text{m}$ in thickness was obtained with a commercial solution. A thin layer of immersion gold ($\sim 0.03 \mu\text{m}$) was plated on the Ni-P to protect the surface from oxidation.

The procedure to form the tensile testing specimens is as follows. First, the surface of Ni-P coatings on each of the Ni plates was coated with rosin mildly activated flux. A Sn-3.5Ag solder wire was rolled into a rectangular-shaped coil of area larger than the joint area (8.0×2.0 mm) of Ni plates in order to supply a sufficient amount of solder for the joining. Two pieces of Ni plates were fixed in a holder, which maintains the opposite ends parallel to each other with a 0.8-mm space between the plates. The specimen setup was sent into a reflow oven and heated at 251°C for 180 seconds and then cooled in air. The excessive solder flowed out of the solder joint area was carefully ground away. The as-soldered specimens were cut into small pieces with rectangular cross section in the dimension of 1.5×2.0 mm using a diamond saw, thus completing the preparation of a tensile testing specimen. The schematic of the tensile testing specimen used in this study is shown in Figure 1.

The as-soldered Sn-3.5Ag/Ni-P tensile testing specimens were thermally aged at 150°C , 170°C , and 190°C for 100, 225, 400, and 625 hours, and at 216°C for 21, 49, and 100 hours. Three samples from each condition were tested.

The tensile test of the solder joints was performed using an Instron 5567 tensile tester (Instron, Boston, MA) at room temperature with a constant crosshead speed of 0.5 mm/min ($8.3 \times 10^{-3} \text{ mm/s}$) to a complete fracture. Force and displacement were recorded during the tests. After the tests, one of the three samples in each condition was mounted and polished to observe the microstructure fracture path on the cross section. A JEOL* JSM-6360A scanning electron microscope (SEM)

*JEOL is a trademark of Japan Electron Optics Ltd., Tokyo.

was used to observe both the cross section of the joint and the top view of the fractured surfaces. The elemental composition of the fracture surfaces was characterized using energy-dispersive X-ray (EDX) analysis with the SEM.

III. RESULTS

In the Sn-3.5Ag/Ni-P reaction, three interfacial layers are formed, as shown in the schematic diagram in Figure 2. Adjacent to the solder is the thickest layer of Ni_3Sn_4 . Two

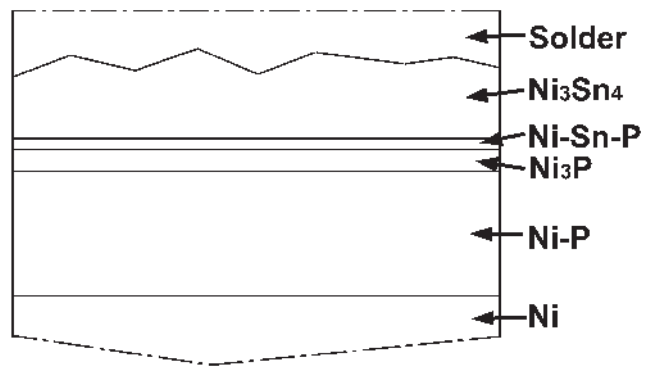


Fig. 2—Schematic diagram of the interfacial layer structure in a thermally aged Sn-3.5Ag/Ni-P solder joint.

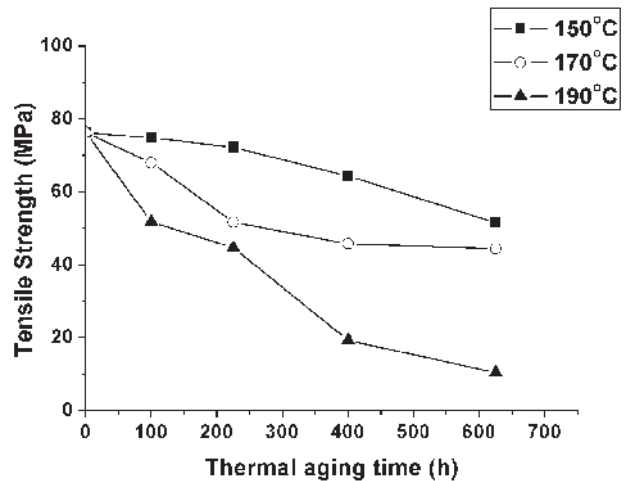


Fig. 3—The degradation of tensile strength for thermally aged Sn-3.5Ag/Ni-P solder joints.

Table I. UTS (MPa) of Sn-3.5Ag/Ni-P Solder Joints After Thermal Aging

Aging Time, Hours	Sn-3.5Ag/Ni-P		
	150 °C	170 °C	190 °C
0	76.3	76.3	76.3
100	74.8	67.9	51.7
225	72.1	51.6	44.6
400	64.3	45.8	19.2
625	51.5	44.3	10.4

thinner layers, Ni-Sn-P and the Ni_3P , are also observed. Discussion of their formation is made elsewhere.^[3]

A. Tensile Strength of Solder Joints

The average ultimate tensile strength (UTS) of the as-soldered Sn-3.5Ag/Ni-P solder joint was 76.3 MPa. Figure 3 depicts the tensile testing results of both as-soldered and thermally aged Sn-3.5Ag/Ni-P solder joints. The tensile strengths of these solder joints aged in different thermal aging processes are also listed in Table I.

From the UTS results in Figure 3, the strength of the Sn-3.5Ag/Ni-P solder joint dropped with the increase of aging temperature and time. The strength degradation was very fast at the aging temperature of 190 °C. Additional tests were performed for specimens aged at 216 °C. It was found that the strength for 21 hours aging was only 7.8 MPa, and further dropped to near zero for 49 and 100 hours of aging.

B. Fracture Surface and Fracture Behavior of Solder Joints

The fractured surfaces were examined to investigate the fracture mechanisms of the tested specimens.

1. As-soldered specimens

Figure 4 is the SEM micrograph showing the cross-sectional view of the complete failure path of as-soldered Sn-3.5Ag/Ni-P solder joint. There was an obvious necking in the bulk solder. The fracture surface was inclined at about

45 deg to the tensile-stress axis. The fractured surface of the broken solder joint is shown in Figure 4(b). Location B in Figure 4(b) lies on the slant plane of the fracture surface inside the bulk solder; therefore, it is not surprising that EDX showed that Sn was the dominant element. Location A in Figure 4(b) is close to the interface. The EDX spectrum in Figure 4(c) verified that this location was also dominated by Sn, indicating that the fracture path is still within the bulk solder. Shallow dimples formed near the edge of the joint were observed, as shown in Figure 5(a). The 45-deg slant fracture surface in Figure 5(b) consisted of small quasi-cleavage facets with many shear lips, indicating a mixture of microscopic brittle and ductile fractures. The EDX analysis shows that the fracture surface contains predominantly Sn. The entire crack is inside the bulk solder in the as-soldered Sn-3.5Ag/Ni-P joint. This shows that the cohesive strength of the interfacial intermetallic compound layer itself and its adhesion to both solder and substrate are stronger than the strength of the bulk solder in the as-reflowed condition.

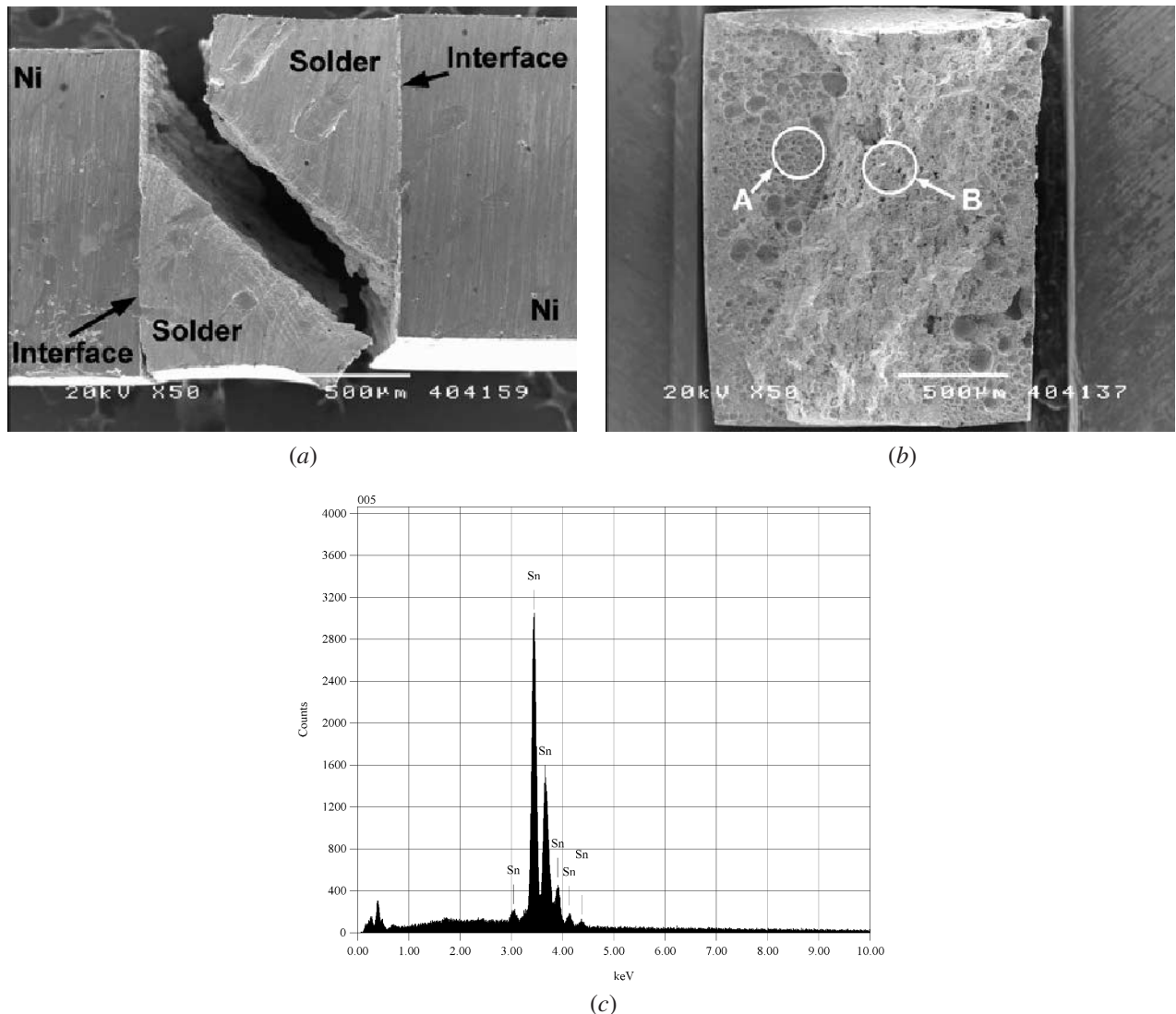
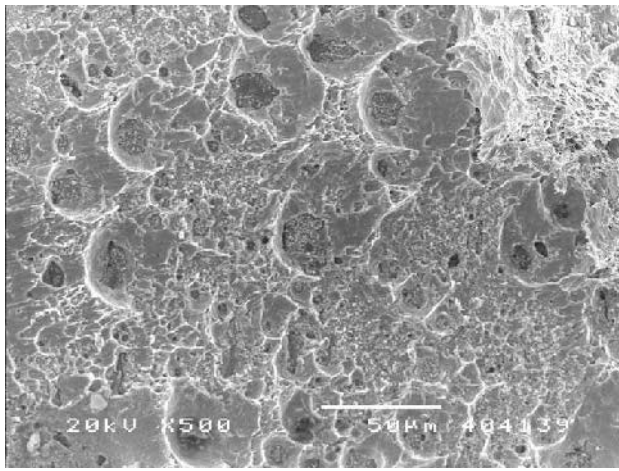
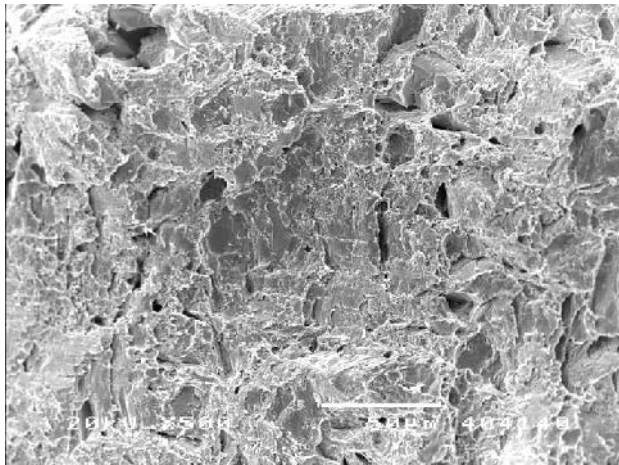


Fig. 4—Failure path and fracture surface of as-soldered Sn-3.5Ag/Ni-P specimens. (a) Cross-sectional view of the entire fracture joint. Notice that necking has occurred in the bulk solder. (b) Fracture surface of the broken solder joint in (a). (c) EDX analysis reveals that Sn dominates at location A shown in (b). An identical result is obtained, but not shown again, at location B. From (a) through (c), it is clear that fracture is completely inside the bulk solder.



(a)



(b)

Fig. 5—Fracture surfaces of as-soldered Sn-3.5Ag/Ni-P solder joint. (a) The part of the fracture surface in circle A in Fig. 4(b). (b) The part of the fracture surface in circle B in Fig. 4(b).

Judging from the amount of necking, the specimen has experienced quite a bit of ductile deformation before fracture.

2. Thermally aged solder joints

For the thermally aged specimens, a general trend was observed for the fracture mode to shift from inside the bulk solder to the interface of the solder joint.

With an aging time of 100 hours at 150 °C, the failure path and fracture surface of the Sn-3.5Ag/Ni-P solder joint were similar to the as-soldered specimens—ductile fracture inside bulk solder. With further extension of aging time, at the same aging temperature, to 225 and 400 hours, the fracture path became a mixed bulk solder and interface failure, and the percentage of failure inside the bulk solder decreased with aging time. When aged for 625 hours, the fracture was completed at the interface, as shown in Figure 6. At 150 °C, the Ni_3Sn_4 IMC thickness for the 625 hours aged sample was 3.7 μm , compared with 2.1 μm in the as-soldered condition.

Figure 7 reveals the fractured surface of the sample aged for 625 hours at 150 °C. From the EDX analysis, failure occurred at the interface between the solder and Ni_3Sn_4 IMC.

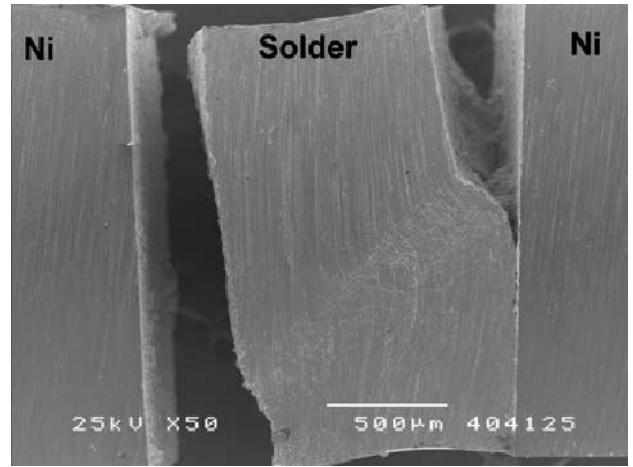
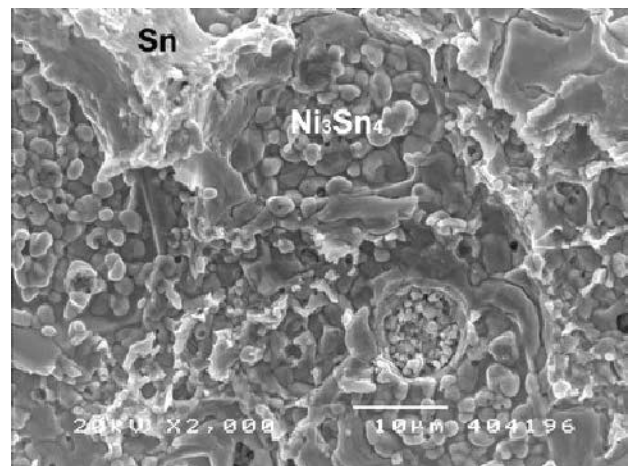
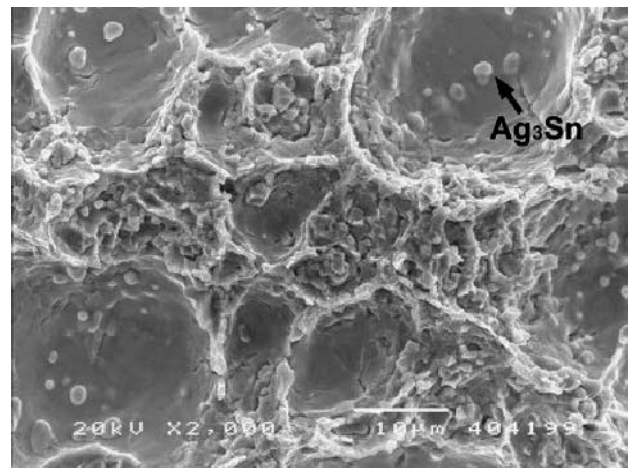


Fig. 6—Failure path of the Sn-3.5Ag/Ni-P solder joint aged at 150 °C for 625 h. Necking and the formation of a shear band in the bulk solder are clearly visible.



(a)



(b)

Fig. 7—Fracture surfaces of Sn-3.5Ag/Ni-P solder joint aged at 150 °C for 625 h: (a) substrate side and (b) solder side.

In this case, large, shallow dimples were present at the IMC/solder interface. Figure 7(a) shows the dimpled surface with the Ni_3Sn_4 IMC in the center of the dimples. Figure 7(b)

shows the fracture surface on the solder side, where the solder with Ag_3Sn particles has been separated from the intermetallic compounds. Further evidence of the interface cracking can be seen from the cross-sectional view of the unbroken side of the solder joint. Figure 8 shows the crack between the solder and Ni_3Sn_4 IMC.

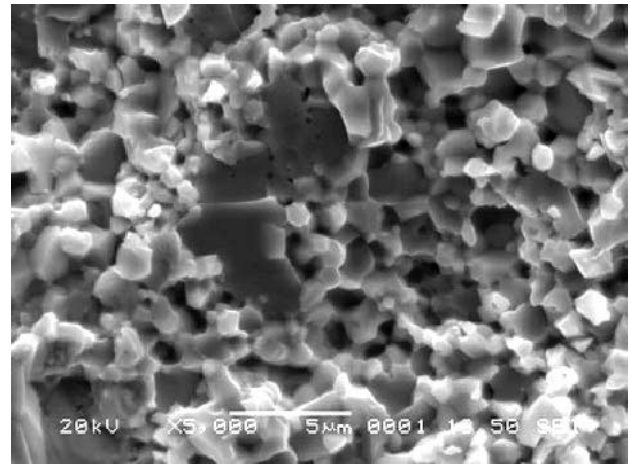
To sum up, in the specimens aged at $150\text{ }^\circ\text{C}$, the fracture is completely interfacial and relatively brittle after 625 hours of aging treatment. For a shorter duration, the fracture is mixed bulk solder failure and interface failure. Necking in the solder still exists in all aged specimens, but the extent is less than in the as-soldered state.

When the Sn-3.5Ag/Ni-P solder joints were thermally aged for 100 hours at $170\text{ }^\circ\text{C}$, failure was predominantly at the solder/ Ni_3Sn_4 interface with a small percentage in the bulk solder. The entire fracture surface was relatively flat, indicating macroscopic brittle behavior. When the aging duration was over 400 hours at $170\text{ }^\circ\text{C}$, the crack still propagated along the interface, and at some locations, it turned into the Ni_3Sn_4 layer, as shown in Figure 9. From the unbroken side of the same solder joint in Figure 9, the crack inside the Ni_3Sn_4 IMC layer could be observed, as shown in Figure 10. Figure 11 shows the fractured surface between the solder and IMC of the sample aged for 625 hours at $170\text{ }^\circ\text{C}$. The crack path was similar to the 400-hour sample, but the interfacial dimples were larger and shallower, indicating increased brittleness at the microscopic scale.

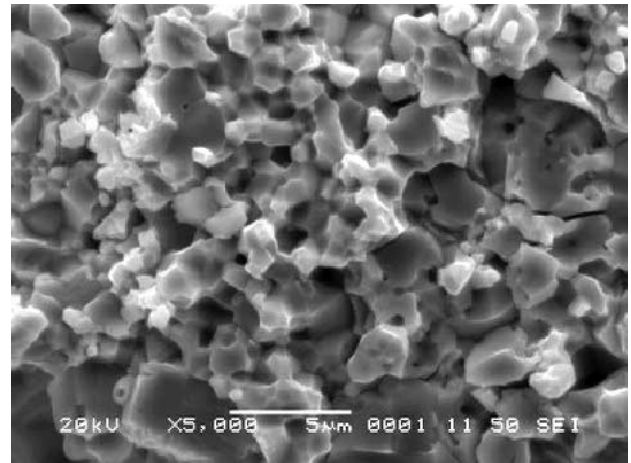
The fracture pattern of the $190\text{ }^\circ\text{C}$ aged samples in Figure 12 was very flat, showing brittle failure in the macroscopic scale. Figure 13 shows the typical microscopic features at the Ni_3Sn_4 /solder interface. The difference with the same interface failed samples aged at $170\text{ }^\circ\text{C}$ is that the dimples became even larger and shallower, which indicates a further loss of ductility compared to the samples aged at lower temperatures.

With further extension of aging time at $190\text{ }^\circ\text{C}$, the fracture did not just stay at the Ni_3Sn_4 /solder interface. At certain locations along the broken interface, the crack propagates through all interfacial layers and reaches the interface of Ni-P coating and its underlying Ni substrate, as shown in

Figure 14. Figure 15(a) shows the cross-sectional view of the position labeled "A" in Figure 14. Kirkendall voids can be observed inside the Ni_3P layer. However, the failure path



(a)



(b)

Fig. 9—Fracture surfaces in Sn-3.5Ag/Ni-P solder joints aged at $170\text{ }^\circ\text{C}$ for 400 h: (a) substrate side and (b) solder side. Both show identical Ni_3Sn_4 IMCs, indicating that the fracture is inside the IMC layer.

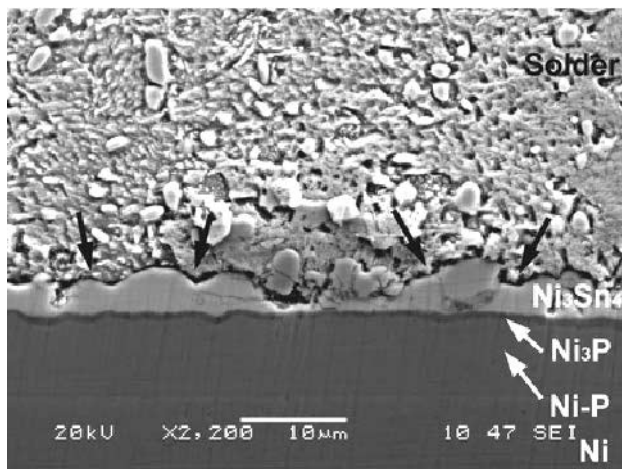


Fig. 8—Black arrows indicate unconnected cracks along the interface between the solder and the Ni_3Sn_4 IMC in the unbroken side of the Sn-3.5Ag/Ni-P solder joint.

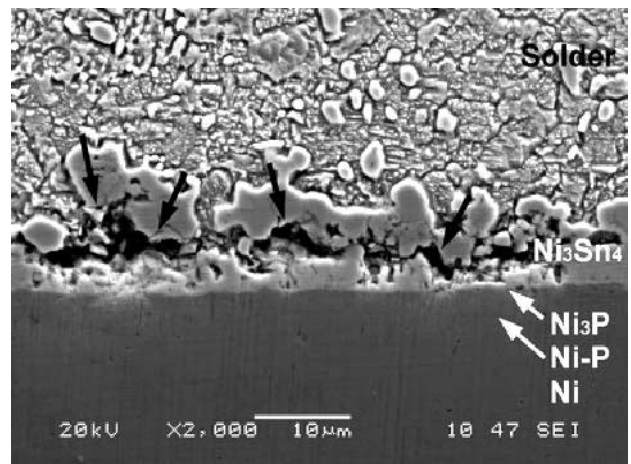
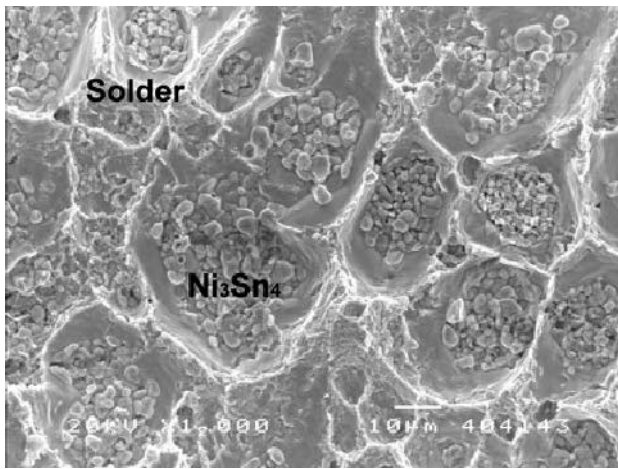
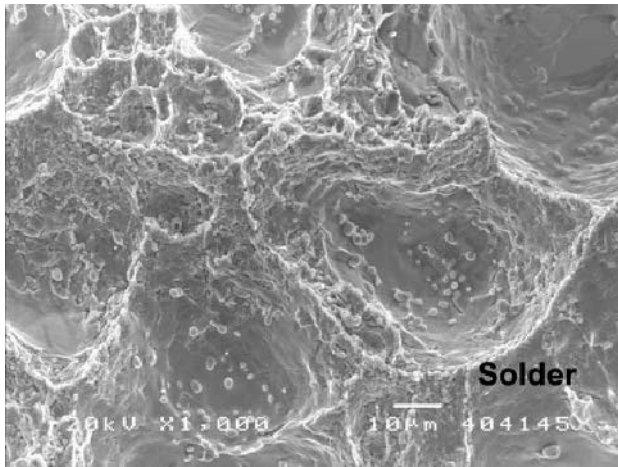


Fig. 10—Cracks (indicated by black arrows) within the Ni_3Sn_4 layer in the unbroken side of the same joint shown in Fig. 9.



(a)



(b)

Fig. 11—Fracture surfaces of the Sn-3.5Ag/Ni-P solder joint aged at 170 °C for 625 h. (a) substrate side and (b) solder side. Separation from the solder/ Ni_3Sn_4 interface is clearly identifiable.

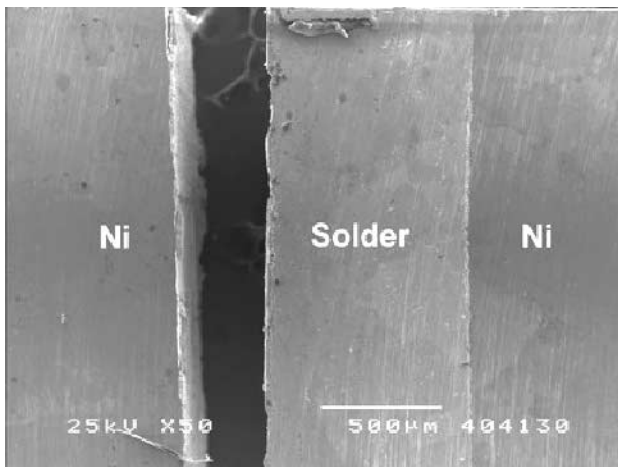
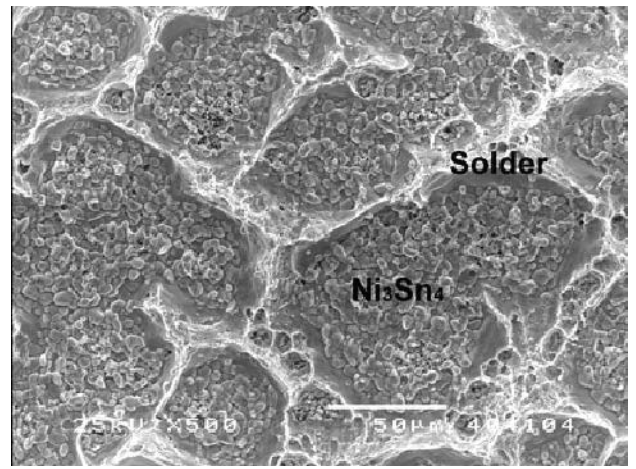
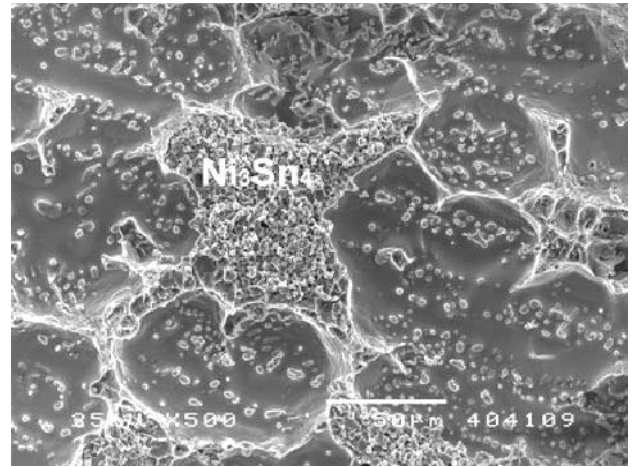


Fig. 12—Cross-sectional view of the failure path in the Sn-3.5Ag/Ni-P specimens aged at 190 °C for 225 h.

was between the solder and the Ni_3Sn_4 IMC. Figure 15(b) shows the portion (labeled “B” in Figure 14) of the crack that ran along the interface between the plated Ni-P coating



(a)



(b)

Fig. 13—Aging for 225 h at 190 °C; the fracture surface through the interface between the Sn-3.5Ag solder and Ni_3Sn_4 . (a) substrate side and (b) solder side.

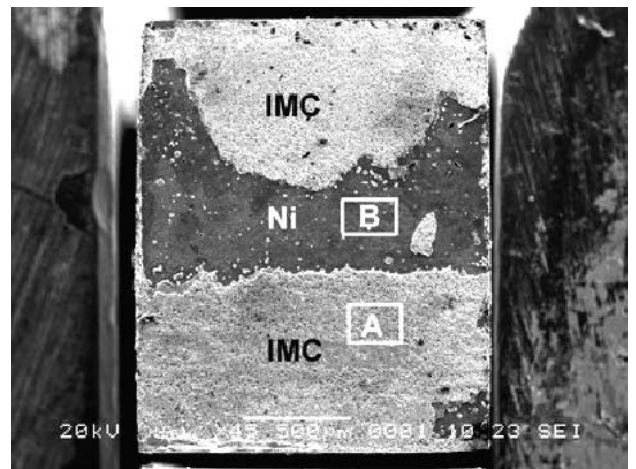
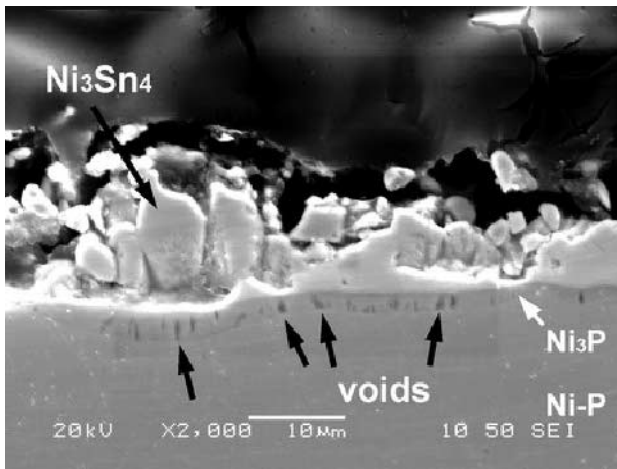
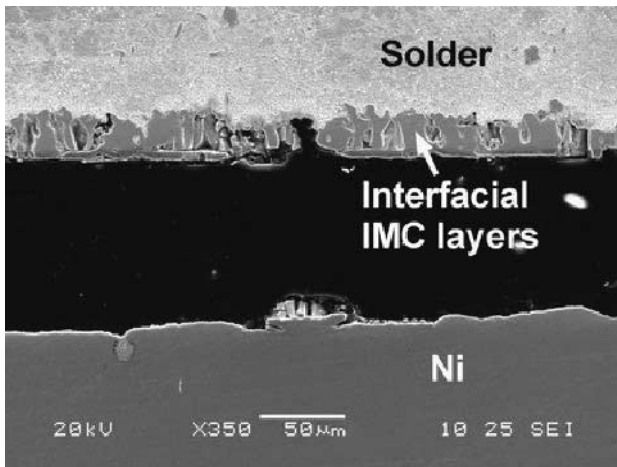


Fig. 14—Fractured surface in the Sn-3.5Ag/Ni-P specimens aged at 190 °C for 400 h, substrate side.

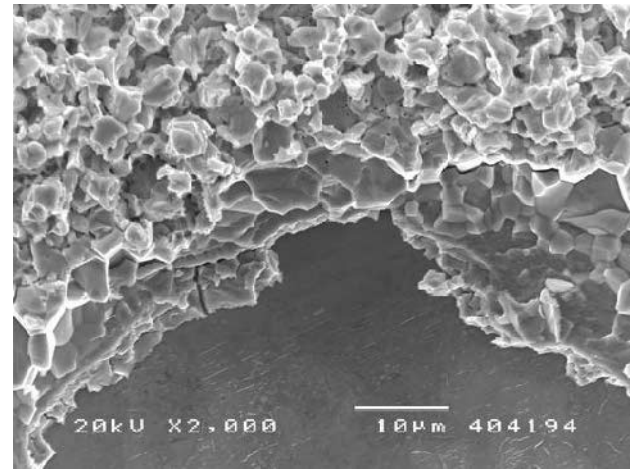
and its Ni substrate. Figure 16(a) is a top view showing the transition of fracture from the solder/ Ni_3Sn_4 interface (on the top) to the Ni-P/Ni interface (bottom). Figure 16(b) reveals



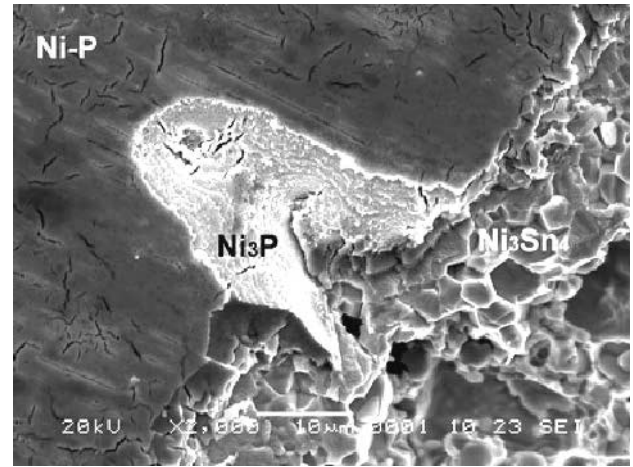
(a)



(b)



(a)



(b)

Fig. 15—Cross-sectional view of the magnified failure path in Fig. 14. (a) The part labeled A is the failure between the solder and Ni_3Sn_4 . Kirkendall voids are visible in the Ni_3P layer. (b) The part labeled B is the failure between the Ni-P and Ni substrate.

Fig. 16—Fracture surface showing that crack propagates through all interfacial layers in the Sn-3.5Ag/Ni-P solder joint aged at 190 °C for 400 h: (a) substrate inside and (b) solder inside.

cracks on the broken Ni-P coating surface, which originally joins the Ni substrate. From the EDX element mapping in Figure 17 and compositional analysis results in Table II, it is further verified that the crack propagates from the interface between the Sn-3.5Ag solder and the Ni_3Sn_4 IMC through the interfacial layers, including the Ni_3Sn_4 , Ni-Sn-P, Ni_3P , and Ni-P coating, eventually reaching the Ni-P/Ni substrate interface. From the cross-sectional view of the unbroken side of the solder joint, cracks could be observed between the Ni-P and Ni substrate, as in Figure 18. The EDX analysis shows that all of the Ni-P had crystallized to Ni_3P where the crack was present. Comparing with the neighboring interface, where the Ni_3Sn_4 and Ni_3P layers are thin, the overgrown interface indeed gives rise to weak strength.

After aging at 190 °C for 625 hours, the entire fracture surface became very flat and shiny under optical microscope. The SEM micrographs of the fracture surface on both the solder and substrate sides are shown in Figure 19. The surface had many “mudflat” cracks on the solder side, as shown in Figure 19(b). From the EDX analysis results, it can be concluded that the failure occurred between the Ni-P coating

layer and the Ni substrate. Aging at 216 °C produced similar results. The strength declined to very low values when mudflat cracks appeared.

IV. DISCUSSION

A. Effect of Thermal Aging on Solder Joint Fracture Behavior

The fracture behavior of Sn-3.5Ag/Ni-P solder joints is strongly influenced by the interfacial reaction during solid-state reaction. The tensile strength of a solder joint is dependent upon all structures in the joint, including the Ni_3Sn_4 intermetallic compound layer and other interfacial layers such as the Ni-Sn-P, Ni_3P , and Ni-P coating. From the observation made in Section III, four typical fracture patterns could be summarized in Figure 20. They are mode I, ductile failure inside the bulk solder; mode II, the dimpled interface failure between the solder and the Ni_3Sn_4 IMC; mode III, failure through interfacial layers (Ni_3Sn_4 , Ni-Sn-P, and Ni_3P); and mode IV, failure between the Ni-P coating and the Ni

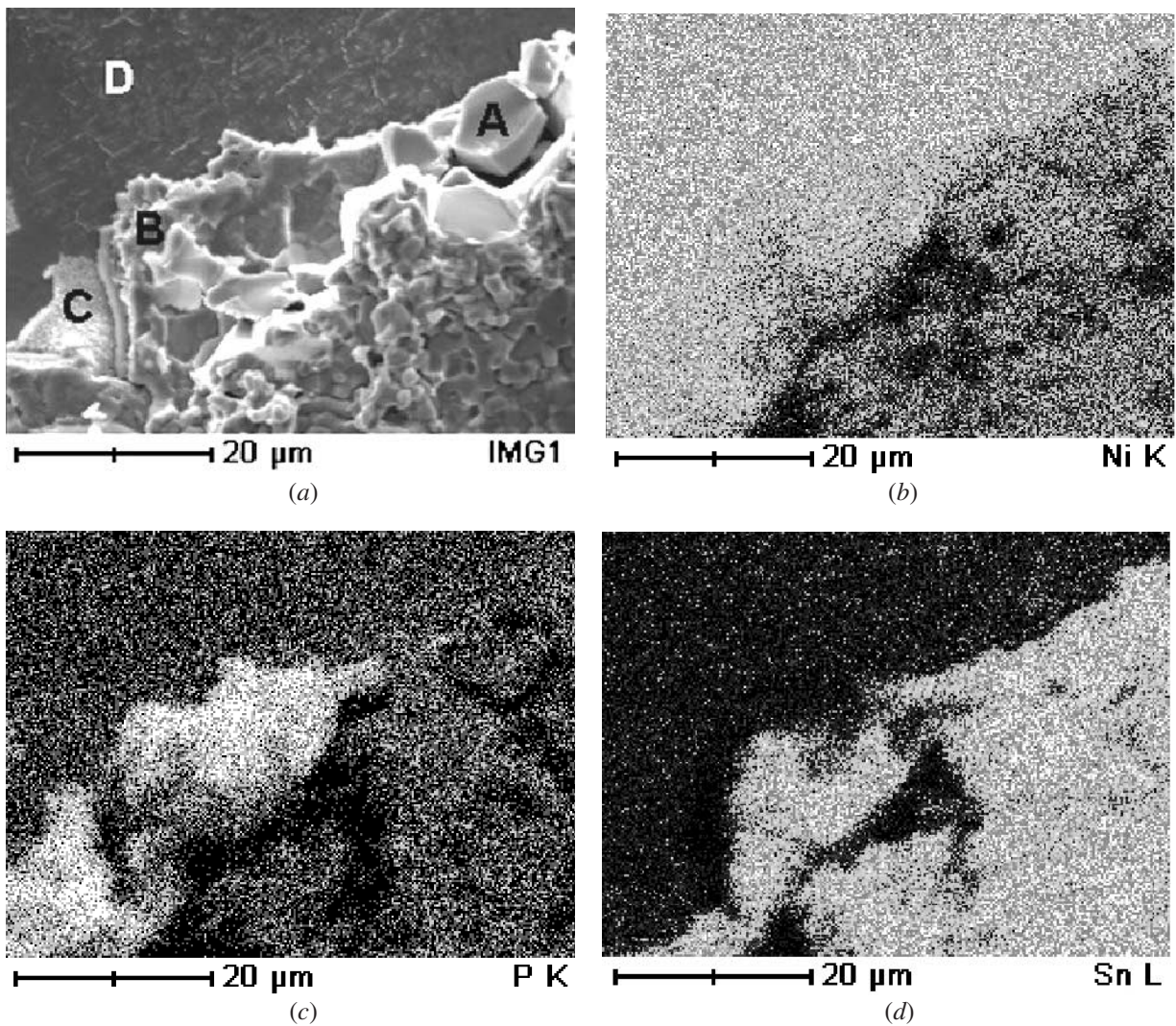


Fig. 17—The EDX element mapping of the fracture surface in the Sn-3.5Ag/Ni-P solder joint aged at 190 °C for 400 h (substrate side). (a) SEM micrograph of the fracture surface, (b) element mapping of Ni, (c) element mapping of P, and (d) element mapping of Sn.

Table II. EDX Results Showing the Composition (Atomic Percent) on the Fracture Surface in Figure 17(a)

Position in Figure	Ni	Sn	P
A (Ni ₃ Sn ₄)	44.45	55.55	—
B (Ni-Sn-P)	56.76	18.16	25.08
C (Ni-P)	78.65	—	21.35
D (Ni)	100	—	—

substrate. The general trend is that with extended aging time and an increase of aging temperature, the fracture mode shifts from mode I to mode IV with decreasing strength. In many cases, mixed modes were observed. A detailed discussion of these failure modes is made subsequently.

In mode I, fracture is inside the bulk solder. Typical examples are shown Figure 4 for the as-soldered joint. The fracture surface shows an obvious dimpled ductile fracture. In this type of solder joint, the deformation is accommodated by the bulk solder rather than the interfacial intermetallics, because the adhesion between the solder and the intermetallic layer is rather strong and can withstand the applied tensile stress. When the solder is deformed, necking occurs with

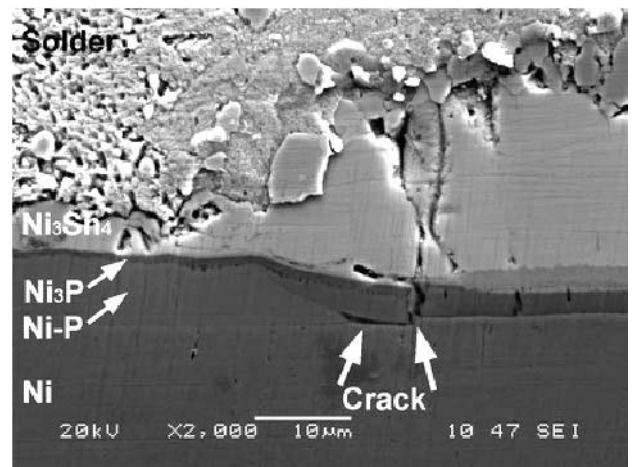
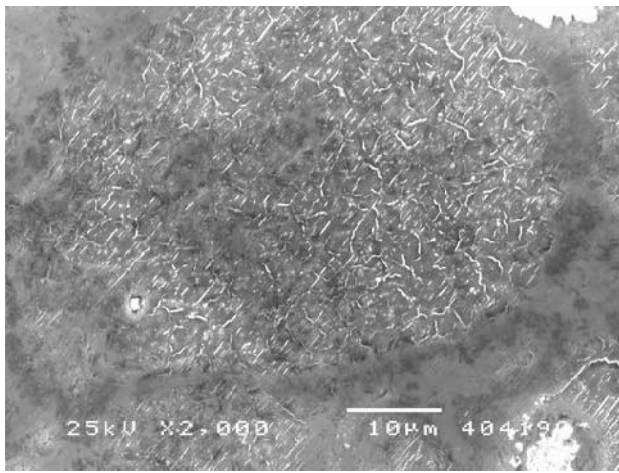
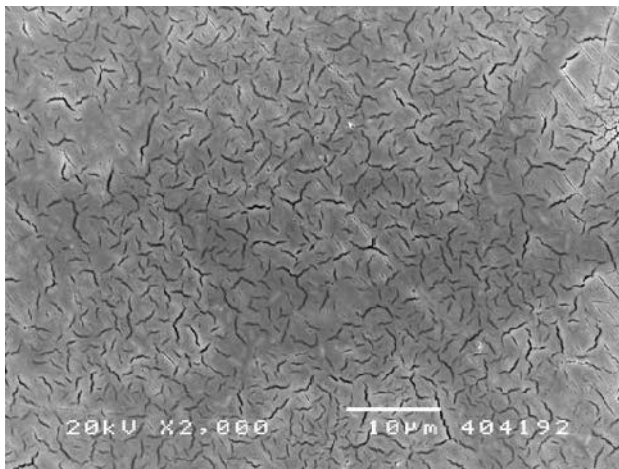


Fig. 18—Crack between Ni-P coating and Ni substrate in the Sn-3.5Ag/Ni-P solder joint aged at 190 °C for 400 h.

increasing plastic strain, and the work hardening around the neck and dimension restrictions result in increasing resistance to deformation. The strain energy is accommodated



(a)



(b)

Fig. 19—SEM micrographs of the fracture surface through the interface between the Ni-P coating and the Ni substrate. Sn-3.5Ag/Ni-P solder joint aged at 190 °C for 625 h. (a) Ni substrate and (b) Ni-P coating layer in solder side.

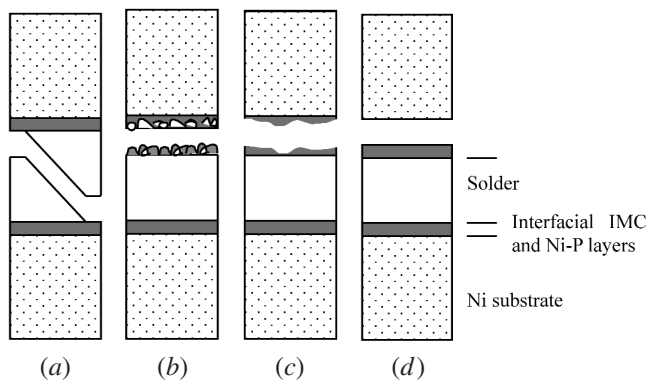


Fig. 20—Schematic plot of the fracture surface in thermally aged Sn-3.5Ag/Ni-P specimens. (a) Mode I: ductile failure inside bulk solder, (b) mode II: dimpled interface failure between solder and Ni_3Sn_4 IMC, (c) mode III: failure through interfacial layers (Ni_3Sn_4 , Ni-Sn-P and Ni_3P), and (d) mode IV: failure between Ni-P coating and Ni substrate.

through deformation and eventual ductile rupture of the bulk solder. The interfacial Ni_3Sn_4 intermetallic compound is relatively thin, only around 2 μm after reflow at 251 °C for 180

seconds,^[3,7] and has not affected the fracture strength of solder joint at this stage.

It is noted that, when the Sn-3.5Ag/Ni-P solder joint fails inside bulk solder, the tensile strength is as high as 76 MPa. Normally, the tensile strength of the bulk Sn-3.5Ag solder is around 30 MPa at room temperature when the strain rate is $1 \times 10^{-3} \text{ s}^{-1}$,^[23] 38 MPa when the strain rate is $2 \times 10^{-3} \text{ s}^{-1}$, and 44 MPa when the strain rate is $16.7 \times 10^{-3} \text{ s}^{-1}$.^[24] In the present study, the strain rate was $10.0 \times 10^{-3} \text{ s}^{-1}$, so the tensile strength of the bulk solder should be in the range of 38 to 44 MPa. Based on the prediction by Cheng and Siewert,^[25] the strength of a free-standing Sn-3.5Ag solder at the current strain rate should be around 40 MPa. However, the tensile strength of the Sn-3.5Ag solder joint is much greater than that of the bulk solder itself. Such an increase in the strength is due to the fact that the deformation of solder in the joint was constrained by the adjacent stronger material. (Note that the thickness of the solder was 0.8 mm on a joint area of $1.5 \times 2.0 \text{ mm}$).

In mode II, the failure path is at the interface between the solder and the IMC layer for thermally aged solder joints; examples are given in Figures 7, 11, and 13. The Ni_3Sn_4 IMC thickness ranges from ~ 3 to $\sim 4 \mu\text{m}$. Dimples appear as a result of the Ni_3Sn_4 IMCs decohesion from the bulk solder. The overall ductility is very limited since deformation is localized at the interface. The reason for the weakening of the Ni_3Sn_4 /solder interface could be due to the stress generated between the IMC and the solder. The stress is caused by the volume mismatch between neighboring layers; the thicker the IMC layer, the larger the stress. Besides, the flattened solder/IMC layer interface in the thermally aged solder joint may also be responsible for the failure path at the interface between the solder and the IMC.^[26] When the IMC thickness exceeds a critical value, the interface becomes weaker than the bulk solder.

In mode III, fracture occurs in one of, or through all of, the interfacial layers. Typical examples are shown in Figures 9 and 16. The Ni_3Sn_4 IMC thickness ranges from ~ 4 to $\sim 5 \mu\text{m}$. The weak interfacial layers may have several causes. The Ni_3Sn_4 IMC is brittle. Therefore, when its thickness grows too large, fracture of the layer itself may occur (Figure 9). A similar observation in other IMCs has been made by other researchers.^[5,9] Stress may be generated due to volume mismatch among the interfacial layers when they grow. From Figure 21, the separation between the Ni_3Sn_4 layer and the layer underneath is clearly revealed. Residual stress, generated by the lattice constant change during IMC formation,^[5] at the interface of the solder and the IMC might also lead to fracture within the IMC.

Kirkendall voids have been cited previously to lead to weakening of the interface by other researchers. The formation mechanisms of Kirkendall voids have been discussed in detail in our previous work.^[3] Jeon *et al.*^[27] used shear testing with a SnPb solder ball on a Ni-P UBM and found Kirkendall voids on the fracture surface after reflow at 250 °C for 16 minutes. So, they attributed the decrease of solder joint strength to the existence of Kirkendall voids. In the current study, however, Kirkendall voids do not appear to have much effect on the fracture of the solder joint under tensile test. There were no Kirkendall voids observed on the fracture surfaces. From the cross-sectional graphs in Figures 15 and 18, Kirkendall voids were clearly visible. However,

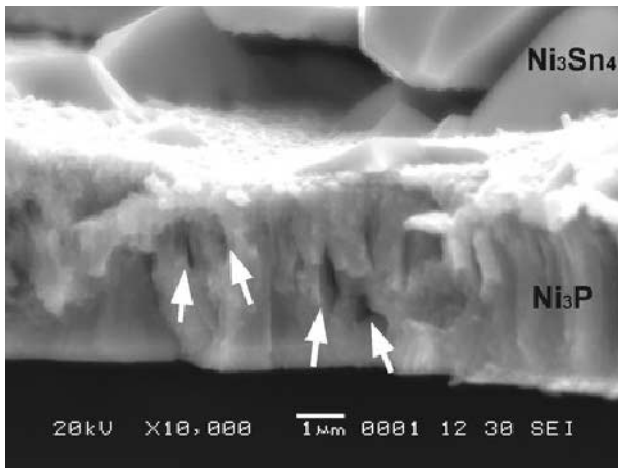


Fig. 21—Crack propagates through all interface layers, including the Ni₃P layer, which contains Kirkendall voids (shown by the arrows). The joint was aged at 190 °C for 400 h.

the cracks were at interfaces rather than inside the Ni₃P layer. Even in the extreme case shown in Figure 21, where they are as large as 1 μm in their long axis, the voids did not act as fracture origination sites. The revelation of the voids was caused by the crack transition from one interface to the other.

Mode IV describes the interface failure between the Ni-P coating layer and the Ni substrate. Examples are shown in Figure 19. The Ni₃Sn₄ IMC thickness is more than 5 μm. When the aging duration is over 400 hours at 190 °C in the Sn-3.5Ag joint, the fracture was by mixed mode III and mode IV. With further increase of the temperature to 216 °C, the entire fracture surface was solely by mode IV. The joint strength was very low. Mudflat cracks could be observed in the fracture surface on the solder side when the Ni-P coating layer peeled away from the Ni substrate, as shown in Figure 19(b). The reason for the mudflat cracks is probably due to the stress caused by the volume change during phase transformation in the Ni-P layer. The density of the original Ni-P (7 wt pct P) coating is 8.2 g/cm³,^[28] and the density of Ni₃P is 7.82 g/cm³.^[20] After Ni-P crystallizes to Ni₃P, the shrinkage is -0.12 pct.^[29] The large volume change could generate high tensile stress in the Ni-P layer to cause the mudflat cracks.^[30] The same stress will also delaminate the Ni-P coating away from the Ni substrate.

B. Relation between Ni₃Sn₄ IMC Thickness and Tensile Strength of Solder Joints

From the analysis in Section A, it can be concluded that during thermal aging, the thickness change of the Ni₃Sn₄ intermetallic layer and formation of other interfacial layers greatly influence the tensile strength and fracture behavior of the Sn-3.5Ag/Ni-P solder joint. A simple indication of the extent of interfacial reaction could be the Ni₃Sn₄ IMC thickness; the thicker the IMC layer, the less the tensile strength. Figure 22 shows the relationship between the IMC thickness and tensile strength of the Sn-3.5Ag/Ni-P solder joints under different thermal aging conditions. The data of Ni₃Sn₄ IMC growth kinetics were discussed in our previous work.^[3] When

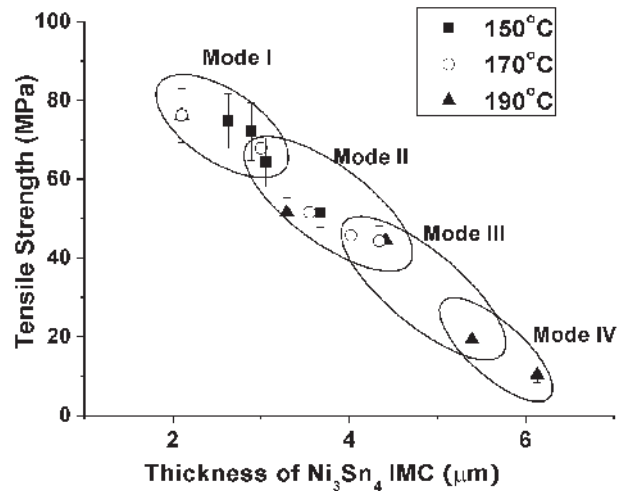


Fig. 22—Failure modes and the relation between the tensile strength and the Ni₃Sn₄ intermetallic thickness of thermally aged Sn-3.5Ag/Ni-P solder joints.

the fracture is inside the solder (mode I), the tensile strength of the Sn-3.5Ag/Ni-P solder joint is always higher than 70 MPa and the thickness of Ni₃Sn₄ IMC is less than 3 μm. When the failure path moves to the interface between the solder and Ni₃Sn₄ IMC (mode II), the tensile strength drops to around 50 MPa and the Ni₃Sn₄ IMC thickness increases to about 4 μm. With mode III, when the failure occurs inside Ni₃Sn₄ and through other interfacial layers, the fracture strength drops significantly to less than 20 MPa. The corresponding Ni₃Sn₄ IMC thickness is more than 5 μm. When the fracture takes place entirely between the Ni-P coating layer and the Ni substrate, the tensile strength is below 10 MPa and the thickness of the Ni₃Sn₄ IMC is more than 6 μm. In the Sn-3.5Ag/Ni-P solder joint, there is an approximately linear correlation between the joint strength and the IMC thickness (Figure 22). Therefore, the IMC thickness inspection could be used as a reliability indication.

V. CONCLUSIONS

In this work, the tensile strength of thermally aged Sn-3.5Ag/Ni-P joints was measured. Fractured surfaces and the failure behavior of these solder joints were analyzed. The effect of intermetallic compounds on the mechanical properties of these solder joints was investigated in detail.

The fracture behavior and failure path of the solder joints change at different thermal aging conditions. Four types of failure modes have been identified in thermally aged Sn-3.5Ag/Ni-P solder joints. They are mode I, ductile failure inside the bulk solder; mode II, dimpled interface failure between the solder and the Ni₃Sn₄ IMC; mode III, failure through interfacial layers (Ni₃Sn₄, Ni-Sn-P, and Ni₃P); and mode IV, failure between the Ni-P coating and Ni substrate. The general trend is that, with extended aging time and increased aging temperature, the fracture mode moves from mode I to mode IV with decreasing strength. In many cases, mixed modes were observed.

The tensile strength of the Sn-3.5Ag/Ni-P solder joints decreases with the extension of aging duration, and the drop becomes very prominent at 190 °C. The thickness of IMCs

provides a good indication of the tensile strength. The reason for such a good correlation is that the thickness variation closely relates to the interfacial reactions on which weakening of the interface is dependent.

Kirkendall voids do not appear to have much effect on the tensile fracture of the joint. This, however, does not rule out possibilities of crack initiation by these voids under other modes of loading, for example, cyclic loading. The volume change of Ni-P phase transformation during the thermal aging process generates high tensile stress inside the Ni-P layer to cause mudflat cracks and delamination of the Ni-P coating.

ACKNOWLEDGMENTS

Financial support from Nanyang Technological University in the form of Academic Research Fund RG19-00 (to ZC) and a research scholarship (to MH) is gratefully acknowledged.

REFERENCES

1. K.N. Tu and K. Zeng: *Mater. Sci. Eng. R*, 2001, vol. 34, pp. 1-58.
2. S. Ahat, M. Sheng, and L. Luo: *J. Mater. Res.*, 2001, vol. 16, pp. 2914-21.
3. M. He, Z. Chen, and G.J. Qi: *Acta Mater.*, 2004, vol. 52, pp. 2047-56.
4. K. Kishimoto, M. Omiya, and M. Amagai: *Proc. 3rd Int. Symp. on Electronic Materials and Packaging*, Cheju, Korea, IEEE, New York, NY, 2002, pp. 8-14.
5. H.T. Lee and M.H. Chen: *Mater. Sci. Eng. A*, 2002, vol. 333, pp. 24-34.
6. T.Y. Lee, W.J. Choi, K.N. Tu, and J.W. Jang: *J. Mater. Res.*, 2002, vol. 17, pp. 291-301.
7. G.J. Qi, M. He, and Z. Chen: *Proc. Yazawa Int. Symp.*, in conjunction with the 2003 TMS Annual Meeting and Exhibition, San Diego, CA, TMS, Warrendale, PA, 2003, vol. 1, pp. 1173-83.
8. M. Amagai, M. Watanabe, M. Omiya, K. Kishimoto, and T. Shibuya: *Microelectron. Reliab.*, 2002, vol. 42, pp. 951-66.
9. D.R. Frear and P.T. Vianco: *Metall. Mater. Trans. A*, 1994, vol. 25A, pp. 1509-23.
10. R.E. Pratt, E.I. Stromswold, and D.J. Quesnel: *J. Electron. Mater.*, 1994, vol. 23, pp. 375-81.
11. R.E. Pratt, E.I. Stromswold, and D.J. Quesnel: *IEEE Trans. Compon. Packaging, Part A*, 1996, vol. 19, pp. 134-41.
12. D.R. Frear, F.M. Hosking, and P.T. Vianco: in *Materials Developments in Microelectronic Packaging*, P.J. Singh, ed., ASM INTERNATIONAL, Materials Park, OH, 1991, pp. 229-40.
13. S.W. Chen, S.W. Lee, and M.C. Yip: *J. Electron. Mater.*, 2003, vol. 32, pp. 1284-89.
14. C.W. Hwang, K. Sukanuma, M. Kiso, and S. Hashimoto: *J. Mater. Res.*, 2003, vol. 18, pp. 2540-43.
15. S.J. Wang and C.Y. Liu: *Scripta Mater.*, 2003, vol. 49, pp. 813-18.
16. K. Zeng and K.N. Tu: *Mater. Sci. Eng. R*, 2002, vol. 38, pp. 55-105.
17. Y.C. Chan, P.L. Tu, C.W. Tang, K.C. Hung, and J.K.L. Lai: *IEEE Trans. Adv. Packaging*, 2001, vol. 24, pp. 25-32.
18. J.W. Jang, P.G. Kim, K.N. Tu, D.R. Frear, and P. Thompson: *J. Appl. Phys.*, 1999, vol. 85, pp. 8456-63.
19. S. Ahat, W. Huang, M. Sheng, and L. Luo: *J. Electron. Mater.*, 2002, vol. 31, pp. 136-41.
20. K.C. Hung, Y.C. Chan, C.W. Tang, and H.C. Ong: *J. Mater. Res.*, 2000, vol. 15, pp. 2534-39.
21. Y. Chonan, T. Komiyama, J. Onuki, R. Urao, T. Kimura, and T. Nagano: *Mater. Trans.*, 2002, vol. 43, pp. 1840-46.
22. Y. Chonan, T. Komiyama, J. Onuki, R. Urao, T. Kimura, and T. Nagano: *Mater. Trans.*, 2002, vol. 43, pp. 1887-90.
23. J.K. Lin, A.D. Silva, D. Frear, Y. Guo, and J.W. Jang: *Proc. 51st Electronic Components and Technology Conf.*, Orlando, FL, IEEE, New York, NY, 2001, pp. 455-62.
24. P.T. Vianco: *Soldering Handbook*, 3rd ed., American Welding Society, Miami, FL, 1999, pp. 214-17.
25. Y.W. Cheng and T.A. Siewert: *J. Electron. Mater.*, 2003, vol. 32, pp. 535-40.
26. D.P. Yao and J.K. Shang: *IEEE Trans. Compon. Packaging, Part B*, 1996, vol. 19, pp. 154-65.
27. Y.D. Jeon, K.W. Paik, K.S. Bok, W.S. Choi, and C.L. Cho: *J. Electron. Mater.*, 2002, vol. 31, pp. 520-28.
28. G.O. Mallory and J.B. Hajdu: *Electroless Plating: Fundamentals and Applications*, Reprint ed., AESF, Noyes/William Andrew Publishing, Norwich, NY, 1990, pp. 122-25.
29. S. Anhock, A. Ostmann, H. Oppermann, R. Aschenbrenner, and H. Reichl: *Symp. on Advanced Packaging Materials*, Braselton, GA, IEEE, New York, NY, pp. 256-61.
30. D. Goyal, T. Lane, P. Kinzie, C. Panichas, K.M. Chong, and O. Villalobos: *Proc. 52nd Electronic Components and Technology Conf.*, San Diego, CA, 2002, pp. 732-39.